

Comparison of Generative Learning Methods for Turbulence Modeling

Claudia Drygala^{1*}, Edmund Ross^{1*}, Francesca di Mare² and Hanno Gottschalk¹

¹*Technical University of Berlin, Institute of Mathematics*

²*Ruhr University Bochum, Department of Mechanical Engineering, Chair of Thermal Turbomachines and Aero Engines
{drygala, ross, gottschalk}@math.tu-berlin.de, francesca.dimare@ruhr-uni-bochum.de*

Abstract

Numerical simulations of turbulent flows present significant challenges in fluid dynamics due to their complexity and high computational cost. High resolution techniques such as Direct Numerical Simulation (DNS) and Large Eddy Simulation (LES) are generally not computationally affordable, particularly for technologically relevant problems. Recent advances in machine learning, specifically in generative probabilistic models, offer promising alternatives for turbulence modeling. This paper investigates the application of three generative models — Variational Autoencoders (VAE), Deep Convolutional Generative Adversarial Networks (DCGAN), and Denoising Diffusion Probabilistic Models (DDPM) — in simulating a 2D Kármán vortex street around a fixed cylinder. Training data was obtained by means of LES. We evaluate each model’s ability to capture the statistical properties and spatial structures of the turbulent flow. Our results demonstrate that DDPM and DCGAN effectively replicate the flow distribution, highlighting their potential as efficient and accurate tools for turbulence modeling. We find a strong argument for DCGAN, as although they are more difficult to train (due to problems such as mode collapse), they gave the fastest inference and training time, require less data to train compared to VAE and DDPM, and provide the results most closely aligned with the input stream. In contrast, VAE train quickly (and can generate samples quickly) but do not produce adequate results, and DDPM, whilst effective, is significantly slower at both inference and training time.

Keywords: Deep convolutional generative adversarial networks, Denoising diffusion probabilistic models, Variational autoencoders, Turbulence modeling, Kármán vortex street

1. Introduction

Turbulent flows are notoriously difficult to model. The structures involved can be found across a wide range of temporal and spatial scales, and the high degree of non-linearity as well as sensitivity to the initial conditions make this an especially challenging problem [1]. In particular, even in the presence of statistical or geometrical symmetries it is not possible to reduce the dimensionality of the problem (e.g. from three- to two- dimensional) in numerical simulations.

Furthermore, these kind of flows play a central role in the field of fluid dynamics, and therefore in diverse fields such as aerospace [2], astrophysics [3], quantum mechanics [4], and even in immune biology [5], since almost all real world flows exhibit turbulence of some kind. Despite the best efforts and decades of research from physicists and mathematicians, a general analytic solution to the governing (Navier-Stokes) equations remains elusive, requiring a variety of computational methods to obtain even numerical solutions. Scale-resolving techniques, such as DNS and LES, strive to resolve the entire spectrum of length and time scales present in the flow, or at least the energetically most significant part (as is the case for LES), whereas conventional averaging approaches (such as Reynolds-averaged Navier-Stokes, or RANS) instead attempt to fit a statistical model. Whilst the former approaches provide the highest possible modelling accuracy, the latter are affected by inevitable loss of information, with non-generalisable closures, strongly affected by flow typology and boundary conditions. Even in techniques such as RANS, which considerably reduce the computational cost of complex simulations, they remain prohibitively high if a large number of computations must be carried out in relatively short time, such as in rapid prototyping and design optimisation loops [6]. This makes the use of machine learning, especially generative probabilistic AI extremely promising, particularly when only statistical distributions resulting from stochastic initial conditions are required [7, 8].

*equal contribution

The availability of large amounts of data, helped by a recent increase in computing power and specialised machine learning hardware, as well as the development of new, bleeding edge model architectures, allow the issue of large computation cost in machine learning to be addressed conveniently, although these are still not remotely comparable to the costs induced by full numerical simulations.

The authors of [9] and [10] pioneered the use of deep neural networks (DNNs) to determine the model constants of nonlinear algebraic vortex viscosity models, significantly improving the prediction of anisotropic turbulence effects.

While early work used machine learning mainly to improve the prediction quality of existing models, also known as ML-augmented turbulence modeling [11, 12, 13, 14, 15, 16, 17, 18], recent publications propose that turbulent flow can be modeled directly by generative models.

In addition to modeling entire flow fields, the applications of generative models range from improving the resolution of flow fields [19], to reconstructing incomplete (gappy) flow fields using the in-painting technique [20], to uncertainty quantification to assess the variability in predictions due to uncertainties in initial or boundary conditions, or indeed in the flow model itself [21, 22].

New generative models are one of the driving forces behind the growing application of generative learning to turbulence modeling. Kingma et. al. [23] introduced the Variational Autoencoder (VAE), a first generative model that provides stochastic variational inference and a learning algorithm that scales to large data sets. Shortly thereafter, Goodfellow et al. [24] proposed a generative adversarial network (GAN) that uses a minimax game to train an optimal generator, providing a paradigm shift in generative learning. Recently, the diffusion probabilistic models (DDPM) was introduced by Ho et. al. [25] as another powerful generative model, which is based on the principle of diffusion models [26] where the distribution of the data is learned by an iterative Markov chain process.

The beauty of all these generative models is that the production of the data at inference time is very inexpensive once the models are trained. This allows for a large volume of data to be created, producing a representation of the target distribution that would be simply impractical to obtain with traditional methods.

The question that remains is whether the results of the generative models are of reasonable quality and which generative model is best suited for modelling 2D turbulence, and in particular, a flow field around a cylinder. We compare three generative models: VAE, Deep Convolutional GAN (DCGAN) [27], and DDPM, and discuss their capabilities and limitations in terms of visual quality, physics-based metrics and computational cost.

Our previous work [28] already showed that GAN-synthesized turbulence match LES-flow excellently. We show in this paper that the DDPM’s results are competitive with GAN, but require significantly more training data, supporting the findings of [29], and are computationally intensive in terms of both training and sample generation. The average inference speed per sample of our DDPM model is 36.3s compared to that of 0.001s by the GAN, a speedup factor of more than 1000. The VAE can generate at 0.0003 samples per second, but suffers from physical and visual inaccuracies.

Outline. The remainder of the paper is structured as follows. Section 2 gives a review on key studies in the field using VAE, GAN or DDPM for applications of turbulence modeling. In section 3 we describe our specific implementation of the VAE, GAN, and DDPM along with a summary of the theoretical foundations of these models. Section 4 offers a brief description of the dataset used in this study. In section 5, we will discuss each model’s performance using physics-based evaluation metrics to assess their effectiveness and examine the associated computational costs. Finally, section 6 will summarize the main findings, discuss their broader implications, and suggest potential avenues for future research.

2. Related work

The review by Zhang et al. [30] gives an overview of the historical development of turbulence modeling approaches, starting with RANS and moving on to LES and modern deep learning methods. In the field of classical simulation methods, RANS can provide solutions at a comparably lower cost, but also paying the penalty of a reduced accuracy. Machine learning approaches represent a promising solution to overcome the problem of high computational cost without losing the details of turbulent structures [31, 32, 33]. In this section we give a broad overview of contributions using VAE, GAN and, DDPM.

Variational Autoencoders (VAE). Over the last few years, modified and extended versions of the Variational Autoencoder have been developed to solve problems in a variety of scientific fields [34, 35, 36, 37, 38]. Advanced VAE frameworks have also been applied to turbulence generation. The authors of [39] presented a

semi-conditional VAE (SCVAE) to reconstruct nonlinear flow from spatially sparse observations, which also allows, due to the probabilistic reconstruction, uncertainty quantification of the prediction. In [40], a two-stage approach is proposed where low-dimensional dynamics reconstructed by an autoencoder are enhanced by another high-resolution neural network. The work of [41] and [42] goes even further and uses a hybrid approach to model turbulence, combining an autoencoder with a multilayer perceptron network or a GAN to predict steady flow fields around supercritical airfoils and nonlinear fluid flows in varying parameterised space.

Generative Adversarial Networks (GAN). Among the new approaches to turbulence modeling, many make use of GAN technology. In our previous work, we introduced GAN as a mathematically well-founded approach for synthetic modeling of turbulent flows [28]. Pioneering this field of research, King et al. [43, 44] showed that GANs are capable of generating syntheses of 2D flow fields after having been previously trained on direct numerical simulation (DNS) data. The reproductions even satisfied statistical constraints of turbulent flows, such as the Kolmogorov - 5/3 law and the small-scale intermittency of turbulence. Using an unsupervised trained combination of a GAN and a recurrent neural network (RNN), Kim and Lee synthesized boundary conditions for turbulent flow [45] or generated stationary DNS flow fields [46].

With the use of more advanced GAN frameworks such as conditional GAN (cGAN), turbulence can be predicted and controlled [47], even only at specific local points [48]. Li et. al. investigated the task of inferring a velocity component from the measurement of a second one for a rotating turbulent flow. To do this, a GAN with context encoders takes the simulated data as input and adds a second loss term that measures the point-to-point distance between the GAN output and the ground truth configuration.

Another application of GAN is the large field of super-resolution reconstruction of turbulent flows. These methods can be used to synthetically scale up low-resolution or noisy flow fields [19, 49, 50, 51, 52, 53, 54, 55]. For these problems, the so-called super-resolution GAN (SRGAN) [56] or enhanced SRGAN (ESRGAN) [57] are used, which can be conditioned by additional physical information [58]. Also the high-fidelity reconstruction of 2D damaged turbulent fields was addressed with GAN [20, 59].

Finally, the generalization capabilities of GAN are of interest and have been investigated. In our previous work, we demonstrated the generalization capabilities of conditional deep convolutional turbulence generators when geometric changes occur in the flow configuration [60]. By changing parameters in the numerical setup, such as the Reynolds number, Nista et. al. investigated the generalization capabilities of their proposed SRGAN [61]. The authors of [62] combined high and low resolution flows to improve the generalization capability for a physics-informed super-resolution GAN (SRGAN).

Denosing Diffusion Probabilistic Models (DDPM). The most recent of the generative models considered in our work are the Denosing Diffusion Probabilistic Models [25] based on the idea of Sohl et. al. [26]. In the field of turbulence modeling, diffusion models are gaining popularity, especially for probabilistic spatiotemporal forecasting. For example, Gao et. al. [63] implemented a Bayesian conditional diffusion model for versatile spatiotemporal turbulence generation. Whereas autoregressive learning with DDPM is often used to solve the task of probabilistic spatiotemporal prediction, cf. [64, 65, 66], Rühling et. al. [67] introduced a dynamically informed diffusion model, which adapts the model to the dynamic nature of the data in order to achieve long-range prediction at inference time. Another application of DDPM in turbulence modeling is the reconstruction of high-resolution turbulent flow fields from low-resolution flow data. For example, Qi et. al. [68] combined a conditional DDPM with an enhanced residual network, and Sardar et. al. [69] developed a preprocessing to decompose flow fields into high and low wavenumber components to learn a conditional DDPM on this data. Furthermore, DDPM were also investigated for training uncertainty-aware surrogate models for simulating turbulence as flows around differently shaped airfoils [70].

3. Methodology

3.1. Variational Autoencoders (VAE)

An autoencoder consists of two components - an encoder $f : \mathcal{X} \rightarrow \mathcal{Z}'$ and a decoder $g : \mathcal{Z}' \rightarrow \mathcal{X}'$ with \mathcal{X} the space of real-world images, \mathcal{Z}' the latent space and \mathcal{X}' the space of reconstructed images. In machine learning, both functions are represented by neural networks, and in our work specifically we use deep convolutional neural networks (DCNN), which are parameterized by weights ϕ and θ . Due to the way an AE is implemented and the definition of its loss function, it can be trained end-to-end. The goal of training an AE is to learn a decoding function that is able to reconstruct an original image from a point in the encoded latent space such that $x' = g_{\theta}(z') = g_{\theta}(f_{\phi}(x)) \approx x$ with $z' \in \mathcal{Z}', x \in \mathcal{X}$ and $x' \in \mathcal{X}'$ (see figure 1). Once

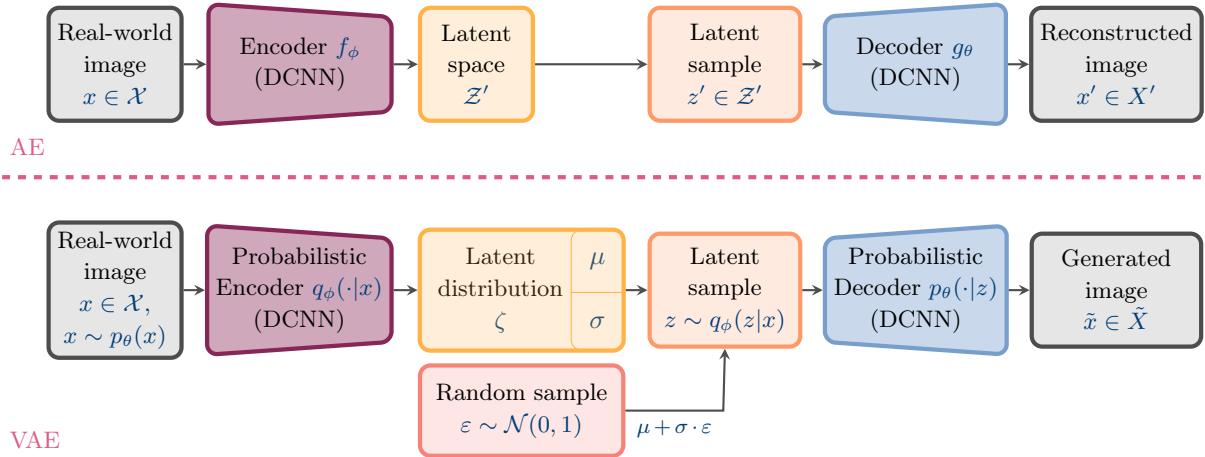


Figure 1: Comparison of the classical [71] (top) and the variational [72] autoencoder (bottom) architectures. In the case of classical AE, the encoder f_ϕ receives as input a real-world image x whose most important features are encoded in the latent space \mathcal{Z}' . Sending a point of this latent space back to the decoder g_ϕ should result in a reconstructed image $x' \approx x$. In contrast, in the case of the VAE, the real images have a chosen distribution, making the encoder and decoder probabilistic. The encoder learns the distribution parameters of the input images, and latent samples are drawn during training by the re-parameterization trick, making it possible to compute the gradients for μ and σ . Due to the stochasticity of the probabilistic decoder’s input, the resulting images are generated rather than reconstructed, as they may differ from the original images.

trained, the process of generating samples, which we also refer to as inference, is a simple matter of picking a point in the latent space and passing it through the decoding function. Typically, the latent space in which important features are embedded is chosen to be small. This property makes AE also a dimensionality reduction method and can be seen as a generalization of principal component analysis (PCA) [73, 71].

In recent years, more advanced variants of the AE have been developed [74], including the variational autoencoder (VAE) [72]. In contrast to a classical AE, the real-world input images $x \in \mathcal{X}$ are drawn from a chosen probability distribution $p_\theta(x)$ parameterized by the network weights θ , making the encoder and decoder probabilistic and the latent space a latent distribution encoding the distribution parameters. In general, this underlying distribution is chosen to be the Gaussian $\mathcal{N}(x; \mu, \sigma)$. Through the application of the powerful mathematical framework of Bayesian probability [75, 76], the VAE can be interpreted as a model of the joint distribution $p_\theta(x, z) = p_\theta(x|z)p_\theta(z)$ of the real-world images $x \in \mathcal{X}$ and the samples of the latent distribution $z \in \zeta$, where the goal is to compute the posterior

$$p_\theta(z|x) = \frac{p_\theta(x|z)p_\theta(z)}{p_\theta(x)} .$$

Here, $p_\theta(x|z)$ is the likelihood of x given z , $p_\theta(z)$ is the prior, and $p_\theta(x) = \int p_\theta(x|z)p_\theta(z)dz$ is the evidence. The problem with the definition of evidence is that its computation requires the evaluation over all possible configurations of latents. This computation is in general expensive and intractable. The solution is to approximate the evidence with a family of distributions $q_\phi(z|x)$, where ϕ are the network weights for the distribution parameters for each data point x . Therefore, a computationally tractable approximation of the posterior can be derived by optimizing the evidence lower bound (ELBO), which leads to the following optimization problem for training the VAE:

$$\arg \min_{\theta, \phi} \mathcal{L}_{\text{VAE}}(x, z; \theta, \phi) = \arg \min_{\theta, \phi} \left[-\mathfrak{D}_{KL}(q_\phi(z|x) || p_\theta(z)) + \mathbb{E}_{z \sim q_\phi(z|x)} \log p_\theta(x|z) \right] , \quad (1)$$

where p_θ and q_ϕ are the probabilistic encoder and decoder respectively and \mathfrak{D}_{KL} is the Kullback-Leibler divergence [77], which quantifies how different $q_\phi(z|x)$ is from $p_\theta(z)$. Note that the right-hand side of (1) shows the reconstruction loss and the left-hand term forces the latent distribution to be close to the Gaussian prior. Since we adopt the ubiquitous assumption of a standard normal prior $p_\theta(z)$ and Gaussian posterior $q_\phi(z|x)$, the KL-divergence can be calculated analytically and only the reconstruction loss needs to be estimated by

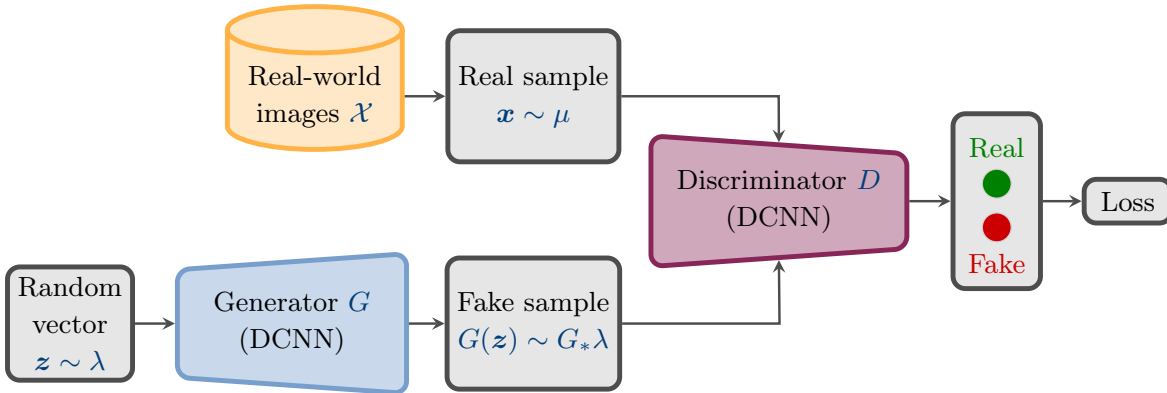


Figure 2: Architecture of a deep convolutional GAN [24, 27]. While the training data is given by the real-world data \mathcal{X} , the fake samples $G(\mathbf{z}) \sim G_*\lambda$ are produced by the generator from a noise vector \mathbf{z} . The discriminator’s inputs are GAN-synthesized and real-world samples, and it’s task is to estimate the probability in a range of $[0, 1]$ that an input sample comes from \mathcal{X} rather than being generated by G . During training, the feedback from the discriminator reaches the generator by backpropagation. The entire GAN framework can be backpropagated at once, since G and D are both fully differentiable and trained end-to-end. If the unknown distribution of the real-world data is approximated by G (i.e. $G_*\lambda \approx \mu$) and D is only able to guess the real-world from the fake samples (i.e. $D(\cdot) \approx 1/2$), the problem (3) reached its optimum.

sampling. Thus, we can rewrite the optimization problem in terms of

$$\arg \min_{\theta, \phi} \left[-\mathfrak{D}_{KL}(q_\phi(z|x) || p_\theta(z)) + \frac{1}{L} \sum_{l=1}^L \log p_\theta(x|z^{(l)}) \right]. \quad (2)$$

With our prior and posterior assumptions, we can simply sample a point z from the standard normal distribution and run it through the trained probabilistic decoder at inference time. However, for sampling at training time, we need to use the so-called reparameterization trick (see figure 1). We want to optimize the distribution parameters μ and σ of the latent distribution ζ from which we want to sample the inputs for the decoder. The problem is that we can’t backpropagate [78] through a stochastic sample because we can’t compute gradients for it. Hence, the idea of reparameterization is to treat μ and σ as deterministic variables, sample a point ε of the standard normal distribution, and define a new latent sample $z = \mu + \sigma \cdot \varepsilon$. With the help of this trick, the stochastic nature of the distribution parameters is disentangled so that we can compute the gradients of μ and σ while still preserving the stochasticity, since \mathbf{z} is also a random variable due to the randomness of ε . Note that since the probabilistic decoder’s inputs are stochastic, the original images are not only reconstructed as in classical autoencoders, but new images can be generated.

3.2. Deep Convolutional Generative Adversarial Networks (DCGAN)

Similar to AE, generative adversarial networks (GAN) are basically composed of two mappings - a generator $G : \Lambda \rightarrow \Omega$ and a discriminator $D : \Omega \rightarrow [0, 1]$, where Λ is the space of latent variables with an easily simulated probability measure λ as Gaussian noise, $\Omega = \{\mathcal{X}, \{G(z)\}\}$ is the space of real-world and generated images, and the interval $[0, 1]$ gives the probability whether a sample is from the real-world images or a generated one. The generator G transforms the noise measure λ to the image measure $G_*\lambda$. The objective of adversarial learning is to train a mapping G using feedback from the discriminator D , such that D cannot differentiate between synthetic samples generated by $G_*\lambda$ and real samples drawn from the unknown target distribution μ . The discriminator D , in turn, is trained as a classifier to assign high probabilities to real-world data and low probabilities to synthesized data. If the generator G has been trained so effectively that even the most optimal discriminator D is unable to distinguish between samples from μ and $G_*\lambda$, then the generative learning process is considered successful, see figure 2.

In practice, both the generator G and the discriminator D are neural networks. The feedback from D to G is propagated backward [78] through the composite mapping $D \circ G$, allowing the neural network weights of G to be updated. Moreover, the universal approximation theorem for (deep) neural networks ensures that any mappings G and D can be approximated to a desired level of precision if the neural networks have a sufficiently wide and deep architecture. For qualitative and quantitative results, see [24, 79, 80, 81, 57, 82]. This work investigates the advanced deep convolutional GAN (DCGAN) [27] framework. As the name

suggests, the generator G and the discriminator D are deep convolutional neural networks (DCNN), which have been successfully applied to image processing [83, 84]. For guidelines on how to properly integrate DCNN into GAN to ensure stable training at high resolution with deeper architecture, see [27].

The training of a GAN is structured as a minimax game between the discriminator D and the generator G , which is mathematically represented by the min-max optimization problem

$$\min_G \max_D \mathcal{L}(D, G) = \min_G \max_D (\mathbb{E}_{\mathbf{x} \sim \mu} [\log(D(\mathbf{x}))] + \mathbb{E}_{\mathbf{z} \sim \lambda} [\log(1 - D(G(\mathbf{z})))]). \quad (3)$$

Note that the loss function $\mathcal{L}(D, G)$ is commonly known as binary cross-entropy [85]. As observed in [24], taking the maximum over a sufficiently large hypothesis space \mathcal{H}_D of discriminators yields to

$$\max_{D \in \mathcal{H}_D} \mathcal{L}(D, G) = \mathfrak{d}_{\text{JS}}(\mu \| G_* \lambda) + \log(4), \quad (4)$$

where, $\mathfrak{d}_{\text{JS}}(\mu \| G_* \lambda)$ is the Jensen-Shannon divergence [86], which is an information-theoretic pseudo-distance between the invariant measure μ and the generated measure $G_* \lambda$ and is defined as

$$\mathfrak{d}_{\text{JS}}(\mu \| G_* \lambda) = \mathfrak{d}_{\text{KL}}\left(\mu \left\| \frac{G_* \lambda + \mu}{2}\right.\right) + \mathfrak{d}_{\text{KL}}\left(G_* \lambda \left\| \frac{G_* \lambda + \mu}{2}\right.\right). \quad (5)$$

Here, the Kulback-Leibler distance between the measures ν and μ is given by $\mathfrak{d}_{\text{KL}}(\mu \| \nu) = -\mathbb{E}_{\mathbf{x} \sim \mu} \left[\log \left(\frac{f_\nu}{f_\mu}(\mathbf{x}) \right) \right]$ with continuous probability densities f_μ and f_ν , respectively. Note that $\mathfrak{d}_{\text{KL}}(\mu \| \nu) = 0$ is only true if and only if $f_\mu(\mathbf{x}) = f_\nu(\mathbf{x})$ with μ -probability one and hence $\mu = \nu$. As a consequence, $\mathfrak{d}_{\text{JS}}(\mu \| G_* \lambda)$ also measures the distance between μ and $G_* \lambda$.

Once trained, the generator is able to synthesize samples from the distribution $G_* \lambda \approx \mu$ by simply sampling a noise vector \mathbf{z} and passing it through G .

Note also that GAN have been shown to be a sound mathematical approach to turbulence modeling, as one can theoretically prove that they converge for ergodic systems. For more details, see our previous work [28].

3.3. Denoising Diffusion Probabilistic Models (DDPM)

Diffusion models convolve the distribution we are interested in into noise via an iterative Markov chain process [26, 25], by adding noise at each timestep. The model then learns the backwards map, that is, the function that returns the noise to the original distribution. The forwards process contains no learnable parameters, and the backwards process is modelled with a neural network, parameterised by weights θ . Figure 3 gives an outline of the model architecture.

3.3.1. VAE Interpretation

Broadly speaking, there are two schools of thought by which to characterise the theory of diffusion models. We will begin with the VAE interpretation, which DDPM also subscribes to. Adapting the minimisation problem 1 from the VAE section above gives

$$\arg \min_{\theta} \left(\mathfrak{d}_{\text{KL}}(q(x_T | x_0) \| p(x_T)) + \sum_{t=1}^T \mathfrak{d}_{\text{KL}}(q(x_{t-1} | x_t, x_0) \| p_\theta(x_{t-1} | x_t)) - \ln p_\theta(x_0 | x_1) \right) \quad (6)$$

Here x_t represents the state of the datapoint x_0 at timestep t in the Markov chain, which has T total steps. x_T is equivalent to the latent variable z , the fully noised datapoint, assumed to be drawn from a standard unit normal with dimension equal to that of the datapoint. The particular implementation used in this paper, denoising diffusion probabilistic models (DDPM) [25], parameterises the forward noising process with a normal distribution

$$q(x_t | x_{t-1}) = \mathcal{N}(x_t; x_{t-1} \sqrt{1 - \beta_t}, \beta_t I) \quad (7)$$

The $\{\beta_t\}$ represent a fixed noise schedule, often linear in t , chosen so that $q(x_T | x_0) \approx \mathcal{N}(0, I)$ [87]. This gives rise to the backwards model, notably also a normal distribution, with analytical form

$$q(x_{t-1} | x_t, x_0) = \mathcal{N}(x_{t-1}; \tilde{\mu}_t(x_t, x_0), \tilde{\beta}_t I) \quad (8)$$

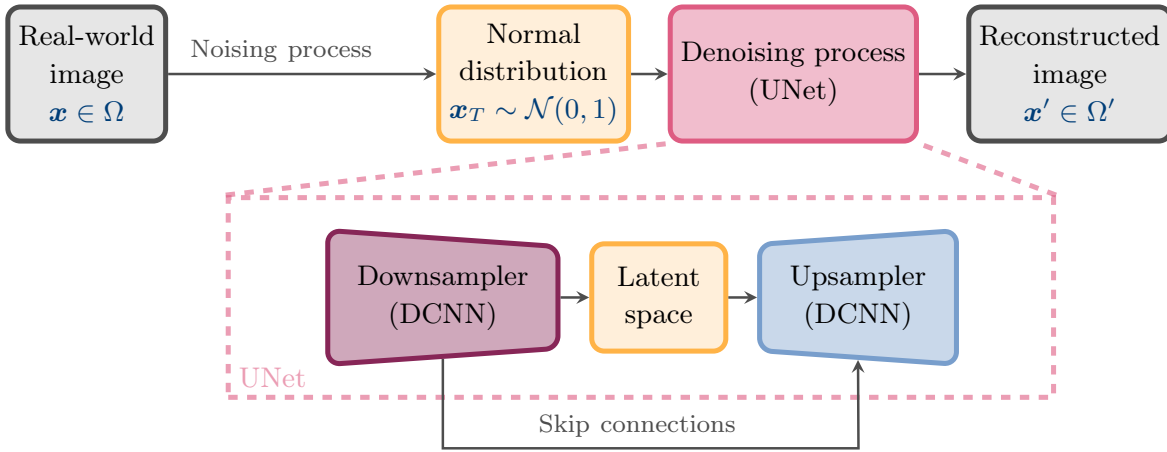


Figure 3: Denoising diffusion probabilistic (DDPM) model architecture [25]. At training time, a sample from the dataset $x \sim \Omega$ is noised to a random step t in the noising process, producing a partially noised sample $x_t \sim \mathcal{N}(x_{t-1}\sqrt{1-\beta_t}, \beta_t I)$. The UNet is trained to produce x_{t-1} from x_t with the parameter t given as a positional embedding. At inference time, a normal sample $x_T = z \sim \mathcal{N}(0, 1)$ is produced and fed to the UNet, which reverses the noising steps one at a time and produces a new sample $x' \sim \Omega'$.

We can do one better and give the forms of $\tilde{\mu}_t(x_t, x_0)$ and $\tilde{\beta}_t$. The full derivation can be found in [88],

$$\tilde{\mu}_t(x_t, x_0) = \frac{\sqrt{\bar{\alpha}_{t-1}}\beta_t}{1-\bar{\alpha}_t}x_0 + \frac{\sqrt{\alpha_t}(1-\bar{\alpha}_{t-1})}{1-\bar{\alpha}_t}x_t \quad (9)$$

$$\tilde{\beta}_t = \frac{1-\bar{\alpha}_{t-1}}{1-\bar{\alpha}_t}\beta_t \quad (10)$$

with the following definitions

$$\alpha_t := 1 - \beta_t, \bar{\alpha}_t := \prod_{s=1}^t \alpha_s \quad (11)$$

We can model this with the generative forward process

$$p_\theta(x_{t-1}|x_t) = \mathcal{N}(x_{t-1}; \mu_\theta(x_t, t), \Sigma_\theta(x_t, t)) \quad (12)$$

and make the choice that $\Sigma_\theta(x_t, t) = \sigma_t^2 I$. We are finally ready to derive the ELBO, as we did with the VAE. Inserting into the minimisation problem 6, and noting that the form of the term in inside the sum can be written [88, 26, 25]

$$\frac{1}{2\sigma_t^2} \|\tilde{\mu}_t(x_t, x_0) - \mu_\theta(x_t, t)\|^2 + C \quad (13)$$

for some C independent of the parameters θ . By itself, this is suitable for optimisation, but we can go one step further, using the reparameterisation trick mentioned in 3.1 [23]. We separate the noise from the data to give

$$x_t(x_0, \epsilon) = \sqrt{\bar{\alpha}_t}x_0 + \epsilon\sqrt{1-\bar{\alpha}_t} \quad (14)$$

where ϵ is distributed with a standard unit (multi-dimensional) normal. It turns out that predicting ϵ leads to better results. Finally, we get

$$\frac{\beta_t^2}{2\sigma_t^2\alpha_t(1-\bar{\alpha}_t)} \|\epsilon - \epsilon_\theta(x_t(x_0, \epsilon), t)\|^2 \quad (15)$$

for our minimisation objective. In practice, we also drop the prefactor since it only scales the loss. In [25] it is noted that, aside from being simpler, this empirically leads to better results.

3.3.2. Continuous Limit

So far we have given the model in terms of discrete Markovian processes, in the sense that

$$x_t = \sqrt{1 - \beta_t}x_{t-1} + \sqrt{\beta_t}\epsilon_t, \quad 1 \leq t \leq T \quad (16)$$

for some ϵ_t , each independently identically distributed by the unit normal. It is natural to ask what happens in the continuous limit, namely as T becomes very large. [87, 89, 90] show that we arrive at the stochastic differential equation (SDE)

$$dX_t = -\frac{1}{2}\beta(t)X_t dt + \sqrt{\beta(t)}dW_t \quad (17)$$

Where $\beta(t)$ is an appropriate continuation of the discrete noise schedule, and W_t is the standard Wiener process. The reverse is also true, as discretising this equation again returns us to the case above [90]. In this sense SDEs can be seen as an overarching framework for diffusion models. Given that the noise schedule increases sufficiently quickly so that $x_T \approx \mathcal{N}(0, I)$, the time reversed (see the main theorem in [91]) SDE is then

$$dY_t = \left(\frac{1}{2}\beta(T-t)Y_t + \beta(T-t)\nabla \log p(x_{T-t}, Y_t) \right) dt + \sqrt{\beta(T-t)}dW_t \quad (18)$$

this is known as a ‘variance preserving’ (VP) SDE. The probability distribution $p(\cdot; x_t)$ (here t is a continuous parameter) satisfies the Fokker-Planck equation, also known as Kolmogorov’s forwards equation, which is an ODE describing how the probability density decays with time [87]. This equation, like equation 18, can be used to sample from the original data distribution [89].

3.3.3. Score-Matching

Another possible interpretation of Diffusion models is to understand them by analogy with score-matching methods, which learn the ‘score’ (the gradient of log probability) with methods such as Langevin dynamics [92]. Note that the score is known for a Gaussian. Indeed, in the formalism we have used so far,

$$\nabla \ln \mathcal{N}(x; \mu, \sigma^2) = \frac{\mu - x}{\sigma^2} \quad (19)$$

Apply the reparameterisation trick from 3.1 to the distribution of x_t and obtain

$$\nabla \ln \mathcal{N}(x_t; \sqrt{\bar{\alpha}_t}x_0, (1 - \bar{\alpha}_t)I) = \frac{\sqrt{\bar{\alpha}_t}x_0 - x_t}{(1 - \bar{\alpha}_t)} = -\frac{\epsilon}{\sqrt{1 - \bar{\alpha}_t}} \quad (20)$$

Learning this score function with mean-squared error leads to the same optimisation problem as 15. Philosophically, this is much the same as models formulated under the VAE interpretation. Where the schools of thought differ is in the noising process (which in turns leads to a different sampling process). SBM (score-based matching) models utilise

$$x_t = x_{t-1} + \sqrt{\sigma_t^2 - \sigma_{t-1}^2}\epsilon_t \quad 1 \leq t \leq T \quad (21)$$

for some noise scales $\{\sigma_t\}$ typically set as a geometric sequence, which again ensure in the limit that the fully noised distribution is equivalent to $\mathcal{N}(0, I)$. Performing the limit procedure above on this process also leads to a SDE, known as a ‘variance exploding’ (VE) SDE, a careful treatment of which can be found in [87].

4. Dataset

4.1. Setup of simulation

We perform our experiments on the test case of a flow around a cylinder at Reynolds number 3900 which is well studied in the literature [93, 94, 95, 93, 96, 97]. The flow field is characterized by a Kármán vortex street developing in the wake of the cylinder. The vortex street consists of a characteristic coherent vortex system in which the rotational axes of the individual vortices are aligned with the cylinder axis.

The data set of grayscale images (see figure 4) was generated by post-processing the transient LES velocity field data using a projection mapping in the sense that the system remains ergodic on a reduced state space. Let $V(\xi, t) = (V_x(\xi, t), V_y(\xi, t), V_z(\xi, t))$ be the velocity field of the fluid. Then for our dataset, the gray scale shows the distribution of the absolute deviation of the local fluctuating velocity magnitude $c(\xi, t) = \sqrt{V_x(\xi, t)^2 + V_y(\xi, t)^2 + V_z(\xi, t)^2}$ at the location ξ from its time average $c'(\xi, t) = |c(\xi, t) - \bar{c}(\xi)|$ with $\bar{c}(\xi) = \frac{1}{T} \int_0^T c(\xi, t) dt$. For the numerical setup of the LES, see [28]. In total, the data set consists of 100,000 images with a resolution of 1000×600 pixels. The full data set is available at [98].



Figure 4: Examples from the dataset of LES simulated flow around a cylinder.

4.2. Computational cost

The LES was run on a partition of the High-Performance Computing (HPC) cluster of the Chair of Thermal Turbomachines and Aero Engines with Intel Xeon “Skylake” gold 6132 CPUs of 2.6 GHz and 96 GB RAM. For the simulation, 20 nodes with 28 cores each had to be allocated and the computation time was about 20 days, which corresponds to 1,440 core weeks.

5. Experiments

5.1. Implementation details

In this work, we investigate VAE and DDPM as alternative generative learning approaches for turbulence modeling and compare them to the DCGAN turbulent flow generator developed in our previous work [28], where the implementation details can also be found. For the training of the VAE and the DDPM, the architecture proposed by [23] and [25], respectively, was adopted. In particular, the VAE consists of an encoder and decoder of similar structure with seven hidden layers containing $\sum_{n=3}^9 2^n$ neurons. We used a more advanced DDPM model with attention, which means it is combined with a transformer [99] and shadowed by an Exponential Moving Average (EMA) model [100]. Both, VAE and DDPM take images of size $m \times m, m \in \mathbb{N}^+$ as input. Therefore, the images were pre-processed prior to training by removing excess white pixels in front of the static wake (150 pixels in the width directory) and by compressing them to a resolution of 512×512 . Finally, all generative networks were built and trained with PyTorch [101]. A summary and comparison of the relevant training parameters, such as learning rate or effective batch size, of the three generative models investigated can be found in table 1.

Model	VAE	DCGAN	DDPM (with attention)
Total Parameters	3,939,085	212,263,362	135,764,353
Layer Sizes	$\{2^n \mid 3 \leq n \leq 9, n \in \mathbb{N}\}$	$\{2^n \mid 4 \leq n \leq 21, n \in \mathbb{N}\}$	$\{2^n \mid 6 \leq n \leq 10, n \in \mathbb{N}\}$
Latent Dim Size	128	100	512×512
Sampling Timesteps	N/A	N/A	1000
Effective Batch Size	512×1	20×1	11×3
Initial Learning Rate	1×10^{-3}	2×10^{-4}	1×10^{-5}
Epochs	150	2,000	200
Optimiser	Adam	Adam	Adam
Use EMA	No	No	Yes
Training Images	100,000	5,000	100,000
Image Resolution	512×512	512×512	512×512

Table 1: Summary of the parameter settings of the generative models VAE, DCGAN and DDPM that were investigated. Note that the effective batch size is the actual batch size multiplied by the gradient accumulation.

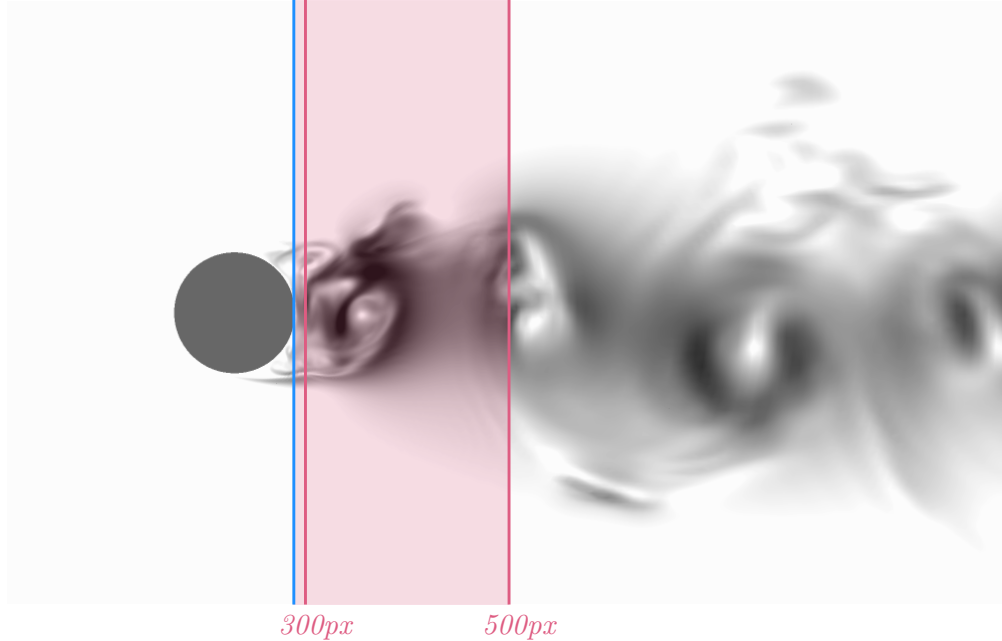


Figure 5: Areas considered for physics-based evaluation. The vertical blue line shows the starting point directly behind the vertebral body. The first reddish vertical line represents the reference line for the small evaluation grid of 12 pixels in x direction away from the starting point (pixel value 300 in the image). The second reddish vertical line describes the reference line for the wide evaluation grid, which inherits 25% of the turbulent flow behind the cylinder (pixel value 500 in the image).

5.2. Physics-based evaluation metrics

To numerically compare the results obtained by the considered generative models, we compute two metrics - the mean pixel values and the variance of the local fluctuating velocity magnitude $c(\xi, t)$ at point ξ - in two areas immediately behind the cylinder, where the strongest statistical fluctuation of the velocities is given (see figure 5). For a detailed description and justification of why these metrics are appropriate for the test case of the flow around a cylinder, see our preliminary work [28]. We performed the evaluations with 5,000 images of the LES and 5,000 images synthesized by the VAE, DCGAN, and DDPM, respectively.

It is worth noting that no known method is capable of reproducing exactly the turbulent flow for a given set of initial conditions, if such a thing even exists, and instead, produce stochastic realisations of what the flow may look like. All of these realisations contain some sort of error, and as such, the models trained on this flawed data will never be able to improve on the error that the data contains. Thus, we do not claim to be able to approximate the flow itself, but rather, we are attempting to approximate the LES data.

5.3. Results Discussion

Figure 6 shows example outputs generated by the three different models, highlighting the variance in quality. The VAE model is clearly the weakest performer, as its generated images are visibly of lower quality compared to those of the other models. It places the wake in the correct position and synthesizes some rough structure of the turbulent flow, but the images are darker, blurred, and lack detail in the vortices. However, when comparing the LES dataset, DCGAN, and DDPM outputs, the differences are not immediately apparent to the naked eye.

Instead, we need to turn to figure 7 and figure 8, which show the physics-based metrics measured along the y -axis over a grid in the x -direction, ending at the 300px and 500px mark, respectively (see figure 5). δ corresponds to the bandwidth of the vortex body, so that y/δ defines the normalized pixel index value of the y -axis. These figures confirm the initial visual assessment, namely, the VAE significantly underperforms, as evidenced by its overprediction of mean pixel values in figure 7a and figure 8a and underprediction of the variation of the pixel values in figure 7b and figure 8b. Clearly, the VAE struggles to accurately represent the statistical properties of the flow.

A noticeable issue with the DCGAN output is the presence of a darkened background in a non-trivial proportion of the images, represented by slightly offset tails in the mean pixel value distributions. The background should be uniformly white (with pixel values exactly zero). This deviation is likely due to the

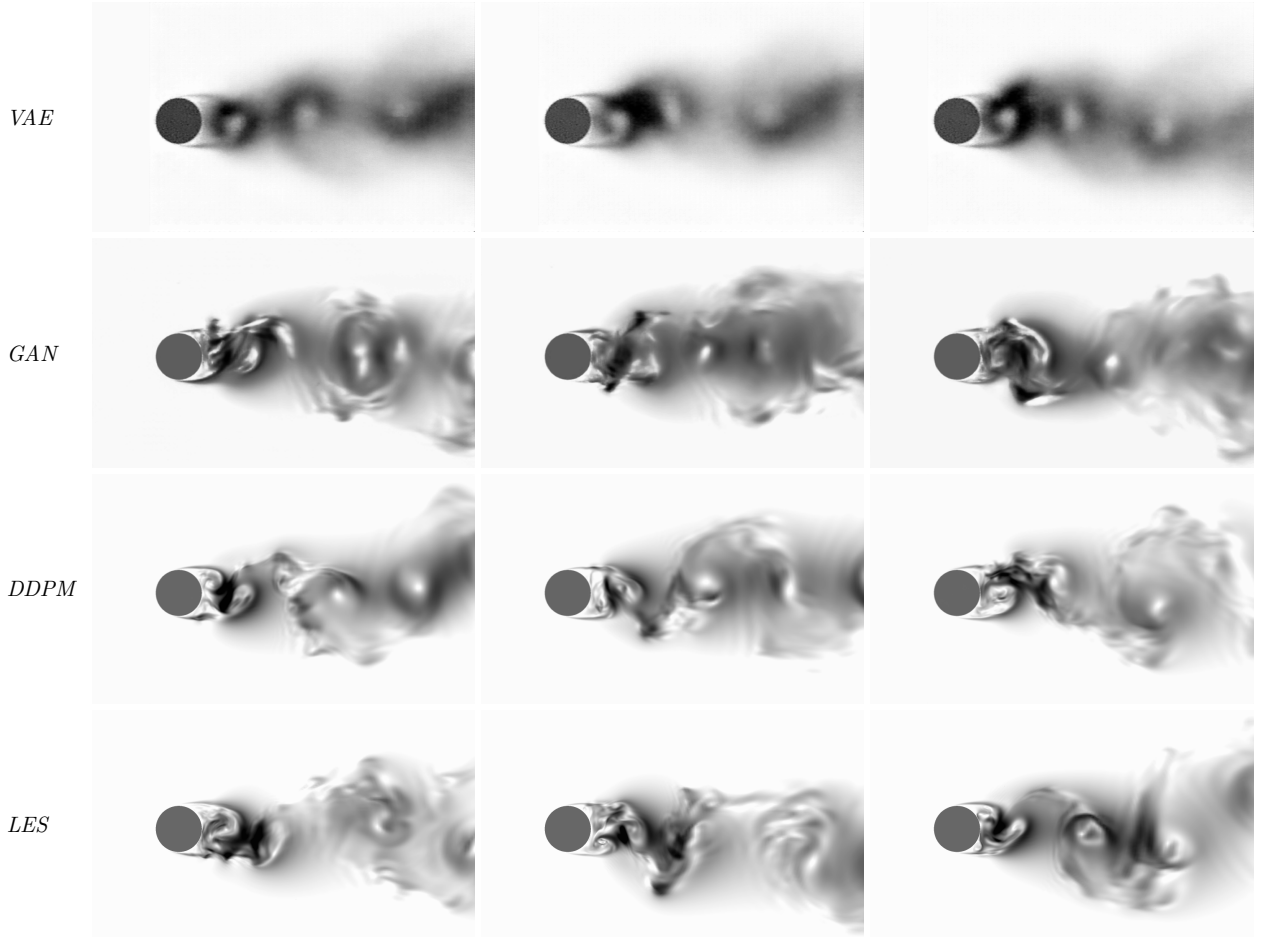


Figure 6: Examples of, from top to bottom, the fully trained VAE, DCGAN, and DDPM, with the LES dataset at the bottom for comparison.

DCGAN’s tendency to prioritize the generation of distinguishable prominent features, sometimes at the expense of accurately capturing uniform background regions, since the discriminator may learn to prioritize these high entropy regions as better predictors of whether or not the image is artificially generated. On top of this, the model inherently introduces noise as part of the generation process. Since the background should be identically zero, the noise can manifest much more noticeably in this region. The DDPM images also suffer from this problem for the same reason, but to a much lesser extent.

Both the GAN and DDPM models exhibit a much better alignment with the dataset with respect to this metric. Despite this, neither model is flawless. The DCGAN somewhat outperforms the DDPM, particularly in capturing the chaotic nature of the flow, since the DDPM tends to underpredict the variation in pixel values, indicating that it has difficulty fully capturing the chaotic turbulence. While the DCGAN also exhibits this underprediction, it does so to a lesser extent. In particular, the GAN better captures the shape of the distributions. An examination of the central region, found in figure 8b, shows that the DCGAN is better able to recreate the “kinks” of the distribution, and in the majority of cases performs better than the DDPM at hitting the peaks.

5.4. Computational Cost

We consider the training and inference time to measure the computational cost (see table 2). Since each of the considered generative models has its own properties, summarized in table 1, each model was trained on different amounts of A100 GPUs with 80GB each.

While VAE and DDPM needed all 100,000 images to train, DCGAN training can be done with 0.05% of the whole dataset without losing generalizability. In addition, the DDPM has over 135 million model parameters. To meet the challenge of a large dataset of high-resolution images and large models, VAE and DDPM were parallelized across multiple GPUs to minimize training time. Note that the speedup for training

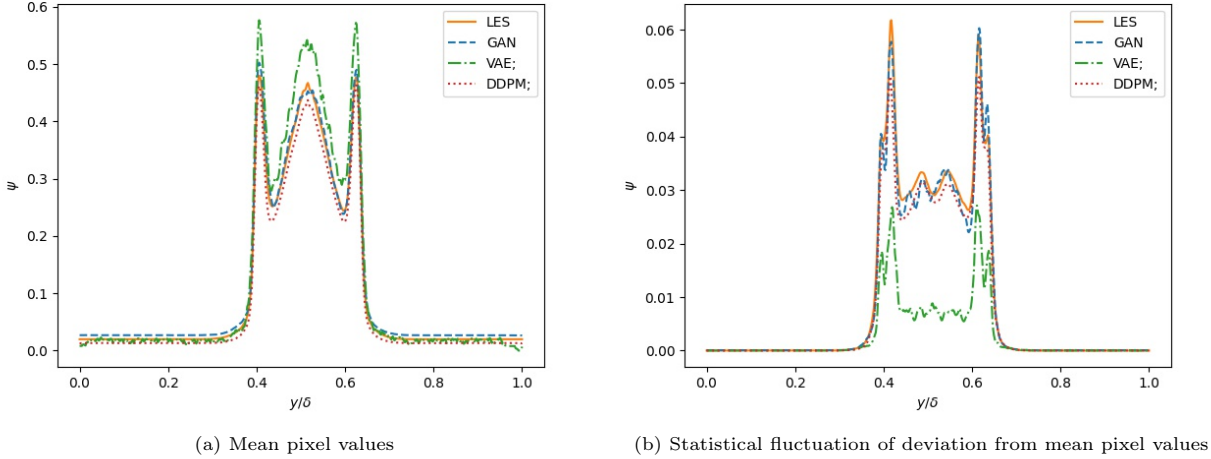


Figure 7: Comparison of (a) the mean pixel values and (b) the statistical fluctuation of the mean pixel values, over the grid ending at the 300px mark (see figure 5). Here, a pixel value represents the difference between the velocity at that point and the background. All datasets were normalized before evaluation.

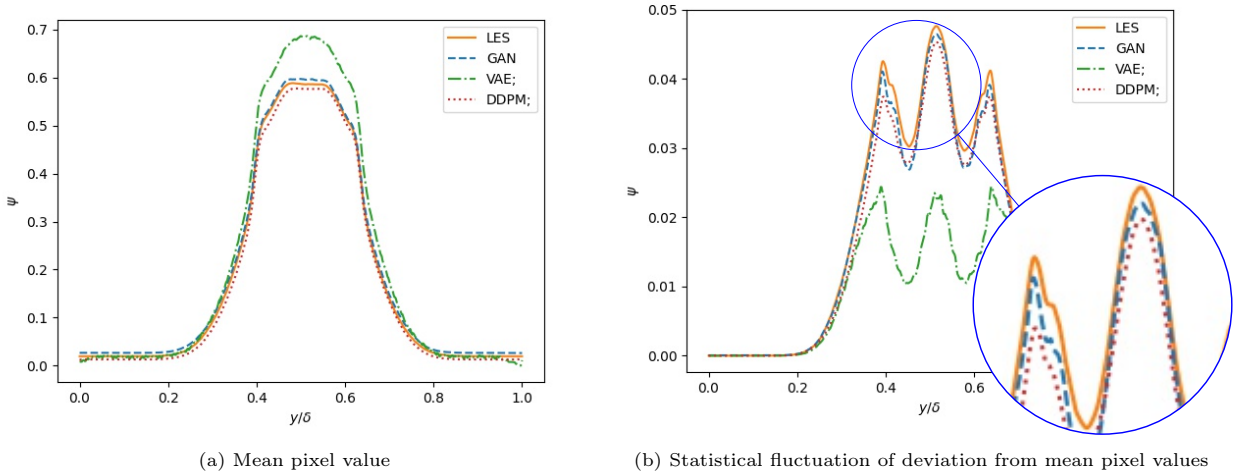


Figure 8: Comparison of (a) the mean pixel values and (b) the statistical fluctuation of the mean pixel values with a zoomed view, over the grid ending at the 500px mark (see figure 5). Here, a pixel value represents the difference between the velocity at that point and the background. All datasets were normalized before evaluation.

with more GPUs in parallel is almost, but slightly less than, linear. Nevertheless, the DCGAN was the fastest to train, despite being the model with the most parameters and being trained over 10 times more epochs than the VAE and DDPM on only one GPU. In terms of inference time, the VAE is significantly faster than the DCGAN and the DDPM, but the generated results don't reach the quality of the LES. Therefore, the inference times of DCGAN and DDPM are of particular interest to us. Here we can see that DCGAN is also significantly faster than DDPM with 0.001 sec/frame compared to 36.3 sec/frame that DDPM needs to generate an image.

Model	VAE	DCGAN	DDPM (with attention)
Training Time	75 hrs total across $4 \times A100$	62 hrs total across $1 \times A100$	490 total hrs across $3 \times A100$
Inference Time	0.000826 sec/frame	0.001 sec/frame	36.3 sec/frame

Table 2: Comparison of the computational cost for the VAE, DCGAN and DDPM.

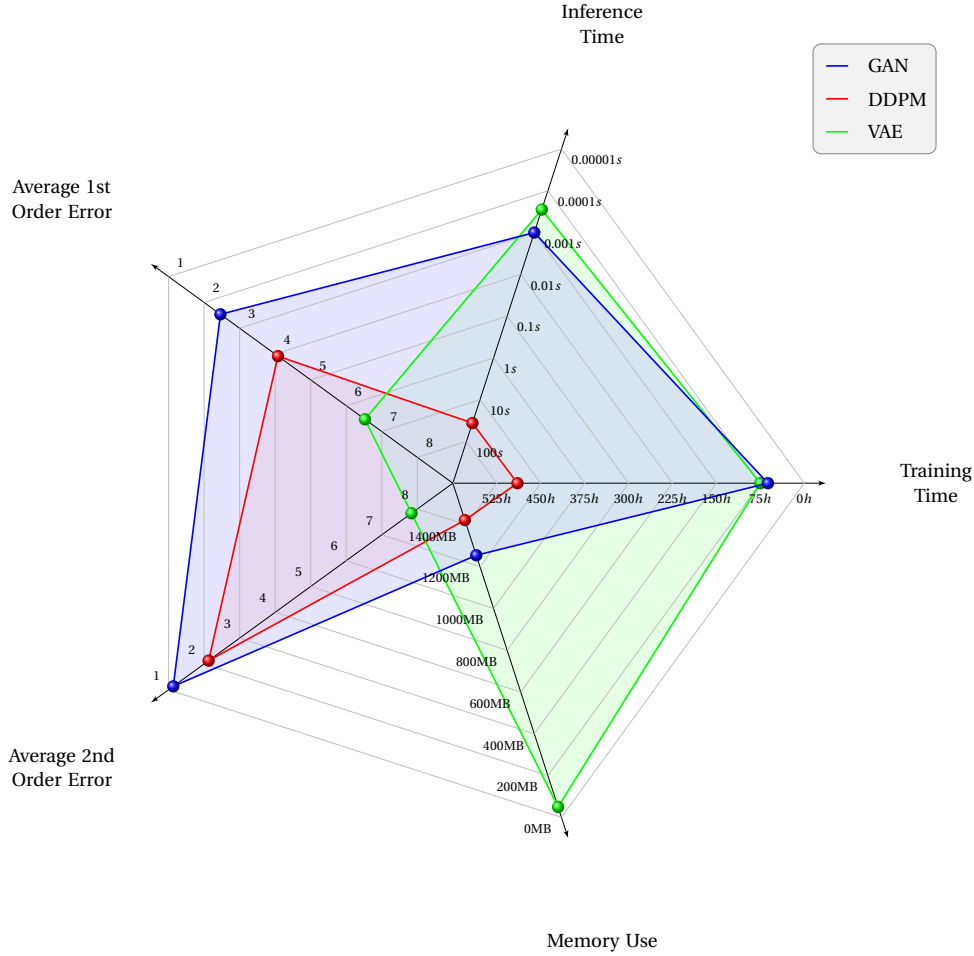


Figure 9: A Kiviati diagram comparing the three generative models. Inference time and memory use are measured per sample, and the errors are measured by taking a mean square error between the respective error curves, and are then placed on a log-scale.

6. Conclusion and Outlook

We compared three generative learning approaches, starting from a VAE, a lighter model with about 4 million parameters, to DCGAN, already widely studied in the field of neural network turbulence modeling, to DDPM, a recent generative model. Our experiments have shown that the VAE is not able to match the quality of the LES, which can be directly observed by just taking a look at the generated image. In contrast, DCGAN and DDPM both synthesize turbulent flow that agrees excellently with the LES flow at the visual level and by examining physics-based metrics. Nevertheless, we found that DCGAN performs better in hitting the peaks of the distributions regarding the physics-based evaluation. Finally, a strong argument for DCGAN was found by analyzing the computational cost, since it requires significantly less data to train and is significantly faster in training and inference time compared to DDPM. In conclusion, figure 9 shows that DCGAN is clearly superior to DDPM, especially in terms of model efficiency. Our experiments have shown that the DCGAN itself, as well as extended variations based on the DCGAN, remain promising for future work in turbulence modeling. However, with the growing amount of data and increasingly powerful computers, DDPM should not be completely discarded for this problem. They are not as efficient as DCGAN, but they are still significantly faster in generating turbulent flow than LES, and the quality is also adequate.

Acknowledgments

This work was funded by the Deutsche Forschungsgemeinschaft (DFG, German Research Foundation) within the priority program "Carnot Batteries: Inverse Design from Markets to Molecules" (SPP 2403) grant no. 526152410.

References

- [1] Uriel Frisch and Andreĭ Nikolaevich Kolmogorov. *Turbulence: the legacy of AN Kolmogorov*. Cambridge university press, 1995.
- [2] P. R. Spalart and V. Venkatakrishnan. On the role and challenges of cfd in the aerospace industry. *The Aeronautical Journal*, 120(1223):209–232, 2016.
- [3] Mark R. Krumholz and Christopher F. McKee. A general theory of turbulence-regulated star formation, from spirals to ultraluminous infrared galaxies. *The Astrophysical Journal*, 630(1):250, sep 2005.
- [4] Carlo F. Barenghi, Ladislav Skrbek, and Katepalli R. Sreenivasan. Introduction to quantum turbulence. *Proceedings of the National Academy of Sciences*, 111(1):4647–4652, mar 2014.
- [5] Abicumarán Uthamacumarán. Cancer: A turbulence problem. *Neoplasia (New York, N.Y.)*, 22:759–769, 10 2020.
- [6] Harish Gopalan, Stefan Heinz, and Michael K Stöllinger. A unified rans–les model: Computational development, accuracy and cost. *Journal of Computational Physics*, 249:249–274, 2013.
- [7] J.L. Lumley. *Stochastic Tools in Turbulence*. Dover books on engineering. Dover Publications, 2007.
- [8] James A. Olson. The motion of fibres in turbulent flow, stochastic simulation of isotropic homogeneous turbulence. *International Journal of Multiphase Flow*, 27(12):2083–2103, 2001.
- [9] Julia Ling, Andrew Kurzawski, and Jeremy Templeton. Reynolds averaged turbulence modelling using deep neural networks with embedded invariance. *Journal of Fluid Mechanics*, 807:155–166, 2016.
- [10] Chao Jiang, Junyi Mi, Shujin Laima, and Hui Li. A novel algebraic stress model with machine-learning-assisted parameterization. *Energies*, 13:258, 01 2020.
- [11] Sai Hung Cheung, Todd A. Oliver, Ernesto E. Prudencio, Serge Prudhomme, and Robert D. Moser. Bayesian uncertainty analysis with applications to turbulence modeling. *Reliability Engineering & System Safety*, 96(9):1137–1149, 2011. Quantification of Margins and Uncertainties.
- [12] W.N. Edeling, P. Cinnella, and R.P. Dwight. Predictive rans simulations via bayesian model-scenario averaging. *Journal of Computational Physics*, 275:65–91, 2014.
- [13] Wouter Edeling, Paola Cinnella, Richard Dwight, and Hester Bijl. Bayesian estimates of parameter variability in the $k - \varepsilon$ turbulence model. *Journal of Computational Physics*, 258:73–94, 02 2014.
- [14] Jack Weatheritt and Richard Sandberg. A novel evolutionary algorithm applied to algebraic modifications of the rans stress–strain relationship. *Journal of Computational Physics*, 325:22–37, 2016.
- [15] J. Weatheritt and R.D. Sandberg. The development of algebraic stress models using a novel evolutionary algorithm. *International Journal of Heat and Fluid Flow*, 68:298–318, 2017.
- [16] Jincheng Zhang and Song Fu. An efficient bayesian uncertainty quantification approach with application to $k - \omega - \gamma$ transition modeling. *Computers & Fluids*, 161:211–224, 2018.
- [17] Weiwei Zhang, Linyang Zhu, Jiaqing Kou, and Yilang Liu. Machine learning methods for turbulence modeling in subsonic flows over airfoils, 06 2018.
- [18] Yaomin Zhao, Harshal D. Akolekar, Jack Weatheritt, Vittorio Michelassi, and Richard D. Sandberg. Rans turbulence model development using cfd-driven machine learning. *Journal of Computational Physics*, 411:109413, 2020.
- [19] Zhiwen Deng, Chuangxin He, Yingzheng Liu, and Kyung Chun Kim. Super-resolution reconstruction of turbulent velocity fields using a generative adversarial network-based artificial intelligence framework. *Physics of Fluids*, 31(12), 2019.
- [20] Qinmin Zheng, Tianyi Li, Benteng Ma, Lin Fu, and Xiaomeng Li. High-fidelity reconstruction of large-area damaged turbulent fields with a physically constrained generative adversarial network. *Physical Review Fluids*, 9(2):024608, 2024.

- [21] Sib0 Cheng, C3sar Quilodr3n-Casas, Said Ouala, Alban Farchi, Che Liu, Pierre Tando, Ronan Fablet, Didier Lucor, Bertrand Iooss, Julien Brajard, Dunhui Xiao, Tijana Janjic, Weiping Ding, Yike Guo, Alberto Carrassi, Marc Bocquet, and Rossella Arcucci. Machine learning with data assimilation and uncertainty quantification for dynamical systems: A review. *IEEE/CAA Journal of Automatica Sinica*, 10(6):1361–1387, 2023.
- [22] Srinivas Soumitri Miriyala, Pramod D. Jadhav, Raja Banerjee, and Kishalay Mitra. 5 - artificial intelligence–based uncertainty quantification technique for external flow computational fluid dynamic (cfd) simulations. In Tilottama Goswami and G.R. Sinha, editors, *Statistical Modeling in Machine Learning*, pages 79–92. Academic Press, 2023.
- [23] Diederik P Kingma and Max Welling. Auto-encoding variational bayes, 2013.
- [24] Ian Goodfellow, Jean Pouget-Abadie, Mehdi Mirza, Bing Xu, David Warde-Farley, Sherjil Ozair, Aaron Courville, and Y. Bengio. Generative adversarial networks. *Advances in Neural Information Processing Systems*, 3, 06 2014.
- [25] Jonathan Ho, Ajay Jain, and Pieter Abbeel. Denoising diffusion probabilistic models, 2020.
- [26] Jascha Sohl-Dickstein, Eric A. Weiss, Niru Maheswaranathan, and Surya Ganguli. Deep unsupervised learning using nonequilibrium thermodynamics, 2015.
- [27] Alec Radford, Luke Metz, and Soumith Chintala. Unsupervised representation learning with deep convolutional generative adversarial networks. In Yoshua Bengio and Yann LeCun, editors, *4th International Conference on Learning Representations, ICLR 2016, San Juan, Puerto Rico, May 2-4, 2016, Conference Track Proceedings*, 2016.
- [28] Claudia Drygala, Benjamin Winhart, Francesca di Mare, and Hanno Gottschalk. Generative modeling of turbulence. *Physics of Fluids*, 34(3), 2022.
- [29] Zhendong Wang, Yifan Jiang, Huangjie Zheng, Peihao Wang, Pengcheng He, Zhangyang Wang, Weizhu Chen, Mingyuan Zhou, et al. Patch diffusion: Faster and more data-efficient training of diffusion models. *Advances in neural information processing systems*, 36, 2024.
- [30] Yi Zhang, Dapeng Zhang, and Haoyu Jiang. Review of challenges and opportunities in turbulence modeling: A comparative analysis of data-driven machine learning approaches. *Journal of Marine Science and Engineering*, 11(7), 2023.
- [31] Jian-Xun Wang, Jin-Long Wu, and Heng Xiao. Physics-informed machine learning approach for reconstructing reynolds stress modeling discrepancies based on dns data. *Phys. Rev. Fluids*, 2:034603, Mar 2017.
- [32] R. Maulik, O. San, A. Rasheed, and P. Vedula. Subgrid modelling for two-dimensional turbulence using neural networks. *Journal of Fluid Mechanics*, 858:122–144, November 2018.
- [33] Varun Shankar, Romit Maulik, and Venkatasubramanian Viswanathan. Differentiable turbulence ii, 2023.
- [34] Irina Higgins, Loic Matthey, Arka Pal, Christopher Burgess, Xavier Glorot, Matthew Botvinick, Shakir Mohamed, and Alexander Lerchner. beta-VAE: Learning basic visual concepts with a constrained variational framework. In *International Conference on Learning Representations*, 2017.
- [35] Bin Dai and David P. Wipf. Diagnosing and enhancing VAE models. *CoRR*, abs/1903.05789, 2019.
- [36] Partha Ghosh, Mehdi S. M. Sajjadi, Antonio Vergari, Michael Black, and Bernhard Sch3lkopf. From variational to deterministic autoencoders, 2020.
- [37] Durk P Kingma, Tim Salimans, Rafal Jozefowicz, Xi Chen, Ilya Sutskever, and Max Welling. Improved variational inference with inverse autoregressive flow. In D. Lee, M. Sugiyama, U. Luxburg, I. Guyon, and R. Garnett, editors, *Advances in Neural Information Processing Systems*, volume 29. Curran Associates, Inc., 2016.

- [38] Aaron van den Oord, Oriol Vinyals, and Koray Kavukcuoglu. Neural discrete representation learning, 2018.
- [39] Kristian Gundersen, Anna Oleynik, Nello Blaser, and Guttorm Alendal. Semi-conditional variational auto-encoder for flow reconstruction and uncertainty quantification from limited observations. *Physics of Fluids*, 33(1):017119, 01 2021.
- [40] Lionel Agostini. Exploration and prediction of fluid dynamical systems using auto-encoder technology. *Physics of Fluids*, 32(6):067103, 06 2020.
- [41] Jing Wang, Cheng He, Runze Li, Haixin Chen, Chen Zhai, and Miao Zhang. Flow field prediction of supercritical airfoils via variational autoencoder based deep learning framework. *Physics of Fluids*, 33(8):086108, 08 2021.
- [42] M. Cheng, F. Fang, C.C. Pain, and I.M. Navon. An advanced hybrid deep adversarial autoencoder for parameterized nonlinear fluid flow modelling. *Computer Methods in Applied Mechanics and Engineering*, 372:113375, 2020.
- [43] Ryan King, Peter Graf, and Michael Chertkov. Creating Turbulent Flow Realizations with Generative Adversarial Networks. In *APS Division of Fluid Dynamics Meeting Abstracts*, APS Meeting Abstracts, page A31.008, November 2017.
- [44] Ryan King, Oliver Hennigh, Arvind Mohan, and Michael Chertkov. From deep to physics-informed learning of turbulence: Diagnostics, 2018.
- [45] Junhyuk Kim and Changhoon Lee. Deep unsupervised learning of turbulence for inflow generation at various reynolds numbers. *Journal of Computational Physics*, 406:109216, 2020.
- [46] Hyojin Kim, Junhyuk Kim, Sungjin Won, and Changhoon Lee. Unsupervised deep learning for super-resolution reconstruction of turbulence. *Journal of Fluid Mechanics*, 910, 2021.
- [47] Jiyeon Kim, Junhyuk Kim, and Changhoon Lee. Prediction and control of two-dimensional decaying turbulence using generative adversarial networks. *Journal of Fluid Mechanics*, 981:A19, 2024.
- [48] Chongyang Yan and Yufei Zhang. Local turbulence generation using conditional generative adversarial networks toward reynolds-averaged navier–stokes modeling. *Physics of Fluids*, 35(10), 2023.
- [49] Kai Fukami, Koji Fukagata, and Kunihiko Taira. Super-resolution reconstruction of turbulent flows with machine learning. *Journal of Fluid Mechanics*, 870:106–120, May 2019.
- [50] Kai Fukami, Koji Fukagata, and Kunihiko Taira. Machine learning based spatio-temporal super resolution reconstruction of turbulent flows, 2020.
- [51] Bo Liu, Jiupeng Tang, Haibo Huang, and Xi-Yun Lu. Deep learning methods for super-resolution reconstruction of turbulent flows. *Physics of Fluids*, 32(2):025105, 2020.
- [52] You Xie, Eric Franz, Mengyu Chu, and Nils Thuerey. Data-driven synthesis of smoke flows with cnn-based feature descriptors. *ACM Transactions on Graphics*, 36(4):1–14, Jul 2017.
- [53] Maximilian Werhahn, You Xie, Mengyu Chu, and Nils Thuerey. A multi-pass gan for fluid flow super-resolution. *Proceedings of the ACM on Computer Graphics and Interactive Techniques*, 2(2):1–21, Jul 2019.
- [54] Mustafa Z. Yousif, Linqi Yu, and Hee-Chang Lim. High-fidelity reconstruction of turbulent flow from spatially limited data using enhanced super-resolution generative adversarial network. *Physics of Fluids*, 33(12):125119, 12 2021.
- [55] Mustafa Z. Yousif, Linqi Yu, and Hee-Chang Lim. Super-resolution reconstruction of turbulent flow fields at various Reynolds numbers based on generative adversarial networks. *Physics of Fluids*, 34(1):015130, 01 2022.

- [56] Christian Ledig, Lucas Theis, Ferenc Huszár, Jose Caballero, Andrew Cunningham, Alejandro Acosta, Andrew Aitken, Alykhan Tejani, Johannes Totz, Zehan Wang, et al. Photo-realistic single image super-resolution using a generative adversarial network. In *Proceedings of the IEEE conference on computer vision and pattern recognition*, pages 4681–4690, 2017.
- [57] Xintao Wang, Ke Yu, Shixiang Wu, Jinjin Gu, Yihao Liu, Chao Dong, Yu Qiao, and Chen Change Loy. Esrgan: Enhanced super-resolution generative adversarial networks. In *Proceedings of the European conference on computer vision (ECCV) workshops*, 2018.
- [58] Akshay Subramaniam, Man Long Wong, Raunak D Borker, Sravya Nimmagadda, and Sanjiva K Lele. Turbulence enrichment using physics-informed generative adversarial networks. *arXiv preprint arXiv:2003.01907*, 2020.
- [59] Tianyi Li, Michele Buzicotti, Luca Biferale, Fabio Bonaccorso, Shiyi Chen, and Minping Wan. Multi-scale reconstruction of turbulent rotating flows with proper orthogonal decomposition and generative adversarial networks. *Journal of Fluid Mechanics*, 971:A3, 2023.
- [60] Claudia Drygala, Francesca di Mare, and Hanno Gottschalk. Generalization capabilities of conditional gan for turbulent flow under changes of geometry. In *Proceedings of the 15th International Conference on Evolutionary and Deterministic Methods For Design, Optimization and Control (EUROGEN 2023)*, 2023.
- [61] Ludovico Nista, CDK Schumann, Temistocle Grenga, Antonio Attili, and Heinz Pitsch. Investigation of the generalization capability of a generative adversarial network for large eddy simulation of turbulent premixed reacting flows. *Proceedings of the Combustion Institute*, 39(4):5279–5288, 2023.
- [62] Mathis Bode, Michael Gauding, Zeyu Lian, Dominik Denker, Marco Davidovic, Konstantin Kleinheinz, Jenia Jitsev, and Heinz Pitsch. Using physics-informed enhanced super-resolution generative adversarial networks for subfilter modeling in turbulent reactive flows. *Proceedings of the Combustion Institute*, 38(2):2617–2625, 2021.
- [63] Han Gao, Xu Han, Xiantao Fan, Luning Sun, Li-Ping Liu, Lian Duan, and Jian-Xun Wang. Bayesian conditional diffusion models for versatile spatiotemporal turbulence generation. *Computer Methods in Applied Mechanics and Engineering*, 427:117023, 2024.
- [64] Dule Shu and Amir Barati Farimani. Zero-shot uncertainty quantification using diffusion probabilistic models. *arXiv preprint arXiv:2408.04718*, 2024.
- [65] Georg Kohl, Liwei Chen, and Nils Thuerey. Benchmarking autoregressive conditional diffusion models for turbulent flow simulation. In *ICML 2024 AI for Science Workshop*, 2024.
- [66] Ruihan Yang, Prakhar Srivastava, and Stephan Mandt. Diffusion probabilistic modeling for video generation. *Entropy*, 25(10):1469, 2023.
- [67] Salva Rühling Cachay, Bo Zhao, Hailey Joren, and Rose Yu. Dyffusion: A dynamics-informed diffusion model for spatiotemporal forecasting. In A. Oh, T. Naumann, A. Globerson, K. Saenko, M. Hardt, and S. Levine, editors, *Advances in Neural Information Processing Systems*, volume 36, pages 45259–45287. Curran Associates, Inc., 2023.
- [68] Jiaheng Qi and Hongbing Ma. A combined model of diffusion model and enhanced residual network for super-resolution reconstruction of turbulent flows. *Mathematics*, 12(7), 2024.
- [69] Mohammed Sardar, Alex Skillen, Małgorzata J Zimoń, Samuel Draycott, and Alistair Revell. Spectrally decomposed diffusion models for generative turbulence recovery. *arXiv preprint arXiv:2312.15029*, 2023.
- [70] Qiang Liu and Nils Thuerey. Uncertainty-aware surrogate models for airfoil flow simulations with denoising diffusion probabilistic models. *AIAA Journal*, pages 1–22, 2024.
- [71] Mark A Kramer. Nonlinear principal component analysis using autoassociative neural networks. *AIChE journal*, 37(2):233–243, 1991.
- [72] Diederik P Kingma. Auto-encoding variational bayes. *arXiv preprint arXiv:1312.6114*, 2013.

- [73] Dana H Ballard. Modular learning in neural networks. In *Proceedings of the sixth National conference on Artificial intelligence-Volume 1*, pages 279–284, 1987.
- [74] Walter Hugo Lopez Pinaya, Sandra Vieira, Rafael Garcia-Dias, and Andrea Mechelli. Autoencoders. In *Machine learning*, pages 193–208. Elsevier, 2020.
- [75] Thomas Bayes. An essay towards solving a problem in the doctrine of chances. *Biometrika*, 45(3-4):296–315, 1958.
- [76] George EP Box and George C Tiao. *Bayesian inference in statistical analysis*. John Wiley & Sons, 2011.
- [77] Solomon Kullback and Richard A Leibler. On information and sufficiency. *The annals of mathematical statistics*, 22(1):79–86, 1951.
- [78] David E. Rumelhart, Geoffrey E. Hinton, and Ronald J. Williams. Learning representations by back-propagating errors. *Nature*, 323:533–536, 1986.
- [79] Hayk Asatryan, Hanno Gottschalk, Marieke Lippert, and Matthias Rottmann. A convenient infinite dimensional framework for generative adversarial learning. *arXiv preprint arXiv:2011.12087*, 2020.
- [80] Ting-Chun Wang, Ming-Yu Liu, Jun-Yan Zhu, Andrew Tao, Jan Kautz, and Bryan Catanzaro. High-resolution image synthesis and semantic manipulation with conditional gans. In *2018 IEEE/CVF Conference on Computer Vision and Pattern Recognition*, pages 8798–8807, 2018.
- [81] Jun-Yan Zhu, Taesung Park, Phillip Isola, and Alexei A Efros. Unpaired image-to-image translation using cycle-consistent adversarial networks. In *Computer Vision (ICCV), 2017 IEEE International Conference on*, 2017.
- [82] Tero Karras, Samuli Laine, and Timo Aila. A style-based generator architecture for generative adversarial networks. In *Proceedings of the IEEE/CVF Conference on Computer Vision and Pattern Recognition*, pages 4401–4410, 2019.
- [83] Saad Albawi, Tareq Abed Mohammed, and Saad Al-Zawi. Understanding of a convolutional neural network. In *2017 International Conference on Engineering and Technology (ICET)*, pages 1–6, 2017.
- [84] Phil Kim. *Convolutional Neural Network*, pages 121–147. Apress, Berkeley, CA, 2017.
- [85] Yaoshiang Ho and Samuel Wookey. The real-world-weight cross-entropy loss function: Modeling the costs of mislabeling. *IEEE Access*, 8:4806–4813, 2020.
- [86] María Luisa Menéndez, JA Pardo, L Pardo, and MC Pardo. The jensen-shannon divergence. *Journal of the Franklin Institute*, 334(2):307–318, 1997.
- [87] Yang Song, Jascha Sohl-Dickstein, Diederik P. Kingma, Abhishek Kumar, Stefano Ermon, and Ben Poole. Score-based generative modeling through stochastic differential equations, 2021.
- [88] Zhifeng Kong, Wei Ping, Jiaji Huang, Kexin Zhao, and Bryan Catanzaro. Diffwave: A versatile diffusion model for audio synthesis, 2021.
- [89] Ling Yang, Zhilong Zhang, Yang Song, Shenda Hong, Runsheng Xu, Yue Zhao, Wentao Zhang, Bin Cui, and Ming-Hsuan Yang. Diffusion models: A comprehensive survey of methods and applications. *ACM Comput. Surv.*, 56(4), November 2023.
- [90] David McAllester. On the mathematics of diffusion models, 2023.
- [91] Brian D.O. Anderson. Reverse-time diffusion equation models. *Stochastic Processes and their Applications*, 12(3):313–326, 1982.
- [92] Yang Song and Stefano Ermon. Generative modeling by estimating gradients of the data distribution, 2020.

- [93] Philippe Parnaudeau, Johan Carlier, Dominique Heitz, and Eric Lamballais. Experimental and numerical studies of the flow over a circular cylinder at reynolds number 3900. *Physics of Fluids*, 20(8):085101, 2008.
- [94] C. Norberg. An experimental investigation of the flow around a circular cylinder: influence of aspect ratio. *Journal of Fluid Mechanics*, 258:287–316, 1994.
- [95] Lawrence Ong and James M. Wallace. The velocity field of the turbulent very near wake of a circular cylinder. *Experiments in Fluids*, 20:441–453, 1996.
- [96] Patrick Bruno Beaudan. *Numerical experiments on the flow past a circular cylinder at sub-critical Reynolds number*. PhD thesis, Stanford University, 1995.
- [97] Arthur G. Kravchenko and Parviz Moin. Numerical studies of flow over a circular cylinder at red=3900. *Physics of Fluids*, 12(2):403–417, 2000.
- [98] Benjamin Winhart and Francesca di Mare. Flow around a cylinder for generative learning, November 2024.
- [99] Ashish Vaswani, Noam Shazeer, Niki Parmar, Jakob Uszkoreit, Llion Jones, Aidan N. Gomez, Lukasz Kaiser, and Illia Polosukhin. Attention is all you need, 2023.
- [100] Tero Karras, Miika Aittala, Jaakko Lehtinen, Janne Hellsten, Timo Aila, and Samuli Laine. Analyzing and improving the training dynamics of diffusion models. *ArXiv*, abs/2312.02696, 2023.
- [101] Adam Paszke, Sam Gross, Francisco Massa, Adam Lerer, James Bradbury, Gregory Chanan, Trevor Killeen, Zeming Lin, Natalia Gimelshein, Luca Antiga, Alban Desmaison, Andreas Kopf, Edward Yang, Zachary DeVito, Martin Raison, Alykhan Tejani, Sasank Chilamkurthy, Benoit Steiner, Lu Fang, Junjie Bai, and Soumith Chintala. Pytorch: An imperative style, high-performance deep learning library. In *Advances in Neural Information Processing Systems 32*, pages 8024–8035. Curran Associates, Inc., 2019.